SAND2016-10885C

Empirically-Derived, Constitutive Damping Model for Cellular Silicone

Jonathan B. Russ
Analytical Structural Dynamics
Sandia National Laboratories
P.O. Box 5800
Albuquerque, NM 87123-0840
jbruss@sandia.gov

Benjamin R. Pacini
Experimental Structural Dynamics
Sandia National Laboratories
P.O. Box 5800
Albuquerque, NM 87123-0557
brpacin@sandia.gov

1 ABSTRACT

One of the more common forms of passive vibration isolation in mechanical systems has been the use of elastomeric or foam pads. Cellular silicone foam is one such example which has been used for vibration isolation and mitigating the effects of mechanical shock. There are many desirable properties of cellular silicone, including its resilience and relative insensitivity to environmental extremes. However, there is very little test data that is useful for understanding its dynamic characteristics or for the development of a predictive finite element model. The problem becomes increasingly difficult since foam materials typically exhibit nonlinear damping and stiffness characteristics. In this paper we present a test fixture design and method for extraction of a few dynamic properties of one type of cellular silicone foam pad. The nonlinear damping characteristics derived from the experimental testing are then used to attempt to improve the predictive capability of a linear finite element model of the system. Difficulties and lessons learned are also presented.

Keywords: cellular silicone, nonlinear damping, foam, strain energy, modal analysis

2 NOMENCLATURE

Symbol	Definition
ω_i	Natural frequency of mode *i*
ζ_i	Damping ratio for mode *i*
$\underline{\underline{M}}$	System mass matrix
$\underline{\underline{C}}$	System damping matrix
$\underline{\underline{K}}$	System stiffness matrix
$\underline{\underline{\Phi}}$	Mode shape matrix
$\underline{\ddot{q}}$	Modal acceleration vector
$\underline{F}$	System external force vector
SE_{CS}	Strain energy in the cellular silicone material
$\underline{\underline{K}}_{CS}$	Cellular silicone stiffness matrix
FEM	Finite element model

3 BACKGROUND

Cellular silicone pads have been commonly used between mechanical components in order to mitigate the effects of vibration and mechanical shock. Typically, the material is also compressed to some extent, either by gravity, bolt loads, or some combination of external loads. As a consequence of the underlying structure of the material and the preload, the material typically exhibits highly nonlinear stiffness and damping characteristics which may significantly impact the dynamics of the overall assembly.

Often it is desirable to be able to predict the response of an assembly to some set of external loads via the use of a finite element model (FEM). Performing testing on real components for all given load cases may be cost prohibitive or perhaps the testing is not currently achievable, either due to lack of knowledge, time, or other constraints. In these cases, development of a mathematical model of the system may be the only option to gain insight into the potential response of a given system.

In an effort to reduce the epistemic uncertainty associated with the development of any model of a physical system, the properties and constitutive models of the materials should be as representative of the physical system as possible. However, this requires sufficient test data that is relevant to and representative of the physics in one's particular system. For common elastic, isotropic materials this is usually not an issue. However, for a material with a more complex behavior, the experimental data in the literature is commonly sparse. This motivates the need for additional material testing.

We will attempt to use experimental modal techniques in conjunction with finite element modeling to derive a constitutive model for the nonlinear damping for cellular silicone pads as a function of strain energy resulting primarily from shear deformation (hereafter referred to as shear strain energy). A test fixture was designed such that the silicone pads were the only medium for energy dissipation within a specified frequency bandwidth. Two sets of impact modal tests were then conducted on this fixture. The first utilized low excitation forces to establish a linear model which was used to initially calibrate a linear FEM of the hardware. The second exercised the nonlinearities in the cellular silicone via high excitation forces. A modal filtering approach similar to that from [1] was used to then extract a time-varying damping function of a specific target mode from this high level excitation data. This nonlinear damping data was then incorporated into a FEM in order to create a constitutive damping model for the cellular silicone material undergoing primarily shear deformation. Note that this constitutive model would only be applicable for determining the damping associated with shear deformation in the silicone. A separate constitutive model would need to be developed to account for the damping associated with compressive/tensile deformation and is included in the plans for future work section of this paper.

In Section 4, the test hardware, instrumentation, and test approach are described along with the results of the low level impact modal test. Section 5 discusses the post-processing of the high level impact data and the method for extracting the time-varying damping. The calibration of the linear FEM for the test hardware to the linear modal results is contained in Section 6. The nonlinear, time-varying damping extracted from the high level experimental data is then incorporated into the FEM as described in Section 7. Using results from the FEM, the damping is then fit in terms of the shear strain energy in the cellular silicone pads. This function is then used to predict the response to different hammer impacts that were conducted on the hardware. Sections 8 and 9 summarize our conclusions and plans for future work.

4 EXPERIMENT

4.1 Test Fixture Design

In an effort to obtain some insight into the dissipative capacity (damping) of the material, a simple test fixture was designed with the intention of isolating the properties of the cellular silicone pad while appropriately representing the base state in which a fifty-percent compression preload is applied. A diagram illustrating the different components of the simple fixture is provided in Fig. 1. The steel block in the center of the fixture is held between the two outer aluminum plates with four rectangular strips of the cellular silicone pads in between. Four bolts pass through the outer aluminum plates allowing the cellular silicone pads to be compressed. In addition, the surfaces of the steel block and aluminum plates that are in contact with the cellular silicone pads were machined to a precise level of surface flatness. In order to accurately control the level of compression of the cellular silicone pads, four steel spacers (hollow cylinders which allow the bolts to pass through) were machined to a precise length. This ensures that when the bolts are sufficiently tightened, the pads will assume the desired level of compression.

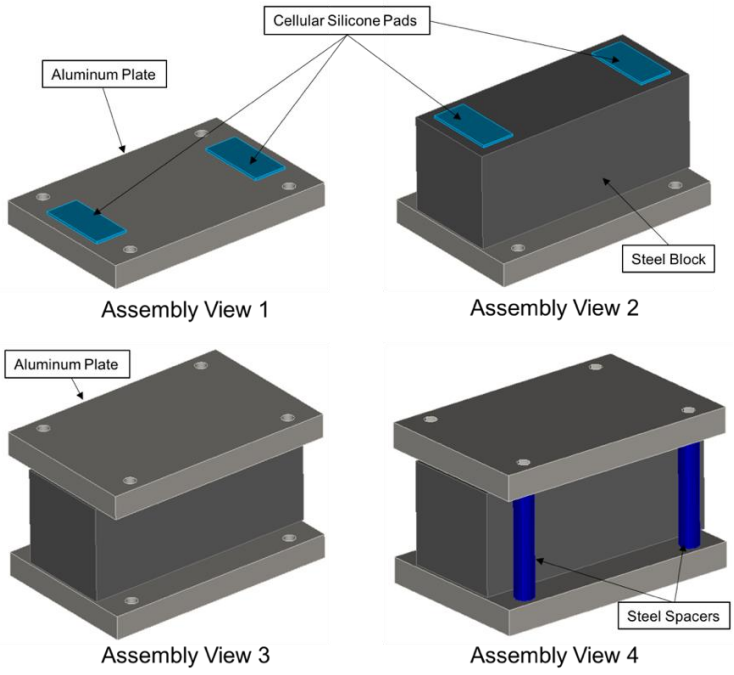

Fig. 1 Test Fixture Assembly Views

The main intent of the test fixture design is to ensure that there will only be strain energy in the cellular silicone material for the first few flexible mode shapes of the system. A "rectangular" shape (i.e. the length of the fixture is longer than its width) was chosen in an effort to better separate the modal frequencies of the first six modes of the system so that extraction of the modal parameters could be performed with higher confidence. The first six mode shapes of the system reflect the rigid body motion of the steel block with respect to the aluminum plates, developing strain energy only in the cellular silicone pads.

4.2 Test Set-Up

The test hardware shown in Fig. 2 was softly suspended using bungee cords to approximate a free-free boundary condition and instrumented with 10 mV/g accelerometers. The accelerometers were located on the block and two plates such that their six degree of freedom (DOF) rigid body modes would be accurately captured: one triaxial accelerometer was placed on each exposed face of the steel block and three uniaxial accelerometers were placed on three orthogonal faces at each corner of each aluminum plate. Additionally, an aluminum cap was placed over the accelerometer on both square faces of the block. These caps allowed for good alignment of the excitation and response when impacting at these locations.

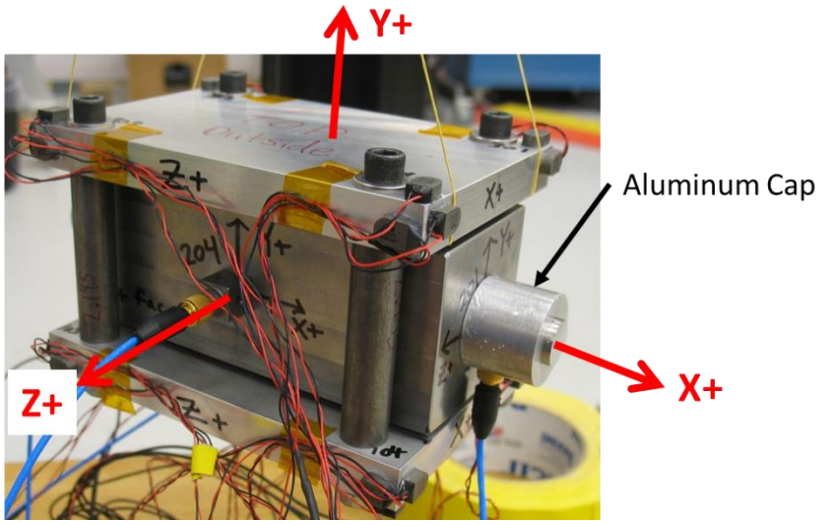

Fig. 2 Test hardware and coordinate system

Two series of hammer impact tests were conducted on this hardware. The first minimized nonlinear response by applying low level inputs with peak forces of approximately 2 N at the locations shown in Table 1. The data from these tests were used to extract the linear model of the hardware. The second set of tests excited nonlinear response of the X-translation mode of the steel block by impacting DOF 201X at 44, 178, and 311 N. The 311 N data was used to extract the nonlinear damping function while the 44 and 178 N data was used to validate the accuracy of this damping function via interpolation using a finite element model. Note that the hammer tip was selected to ensure that the excitation bandwidth only included the rigid modes of the steel block with respect to the fixture and not the elastic fixture modes. This ensures that all strain energy is contained in the silicone pads.

Table 1 Excitation Information

Input DOF	Description	Low Level Peak Force (N)	High Level Peak Force (N)
101Z	Lateral input at corner of lower plate	2	N/A
201X	Lateral input on square face of steel block	2	44, 178, 311
303Y	Vertical input at corner of upper plate	2	N/A
304Y	Vertical input at corner of upper plate	2	N/A

4.3 Linear Modal Analysis Results

The Synthesize Modes And Correlate (SMAC) program by Mayes and Hensley [2] was used to extract the modal parameters from the low level impact data using a real modes approximation in Table 2. Rigid body mode shapes were calculated from the measured physical properties of the hardware.

Table 2 Linear Modal Parameters[1,2]

Mode	Frequency (Hz)	Damping (%cr)	Reference	Description
7	93	6.37	101Z	Block translation in global Z with rotation in Y-Z plane (roll mode)
8	106	5.98	201X	Block translation in global X
9	116	6.24	101Z	Block rotation in X-Z plane (yaw mode)
10	127	6.12	101Z	Block rotation in Y-Z plane (roll mode) with translation in global Z
11	190	11.91	304Y	Block translation in global Y
12	209	10.28	303Y	Block rotation in X-Y plane (pitch mode)

[1]Rigid body modes not shown

[2]Highlighted mode is the target mode for nonlinear analysis

These data were used to create the mode shape matrix that is utilized later in this report. The X-translation mode of the block (mode 8) is the target mode for the nonlinear analysis as it deforms the silicone pads purely in shear. Additionally, it is the mode that is able to be most purely excited given the test fixture and instrumentation.

5 POST-PROCESSING OF HIGH LEVEL IMPACT DATA

The objective for this work is to develop a nonlinear damping function in terms of cellular silicone shear strain energy. Simple shear in the pads is achieved when the steel block rigidly translates in the X-direction (mode 8 from Table 2). The next step is to extract the nonlinear, time-varying damping of this mode. This is accomplished in two phases. The first phase is to extract the motion of mode 8 from the responses measured by the accelerometers during the 311 N impact test. This is accomplished using a modal filter. The second task is the calculate the time-varying damping of this mode. The following two subsections discuss these processes in further detail.

5.1 Modal Filter

The use of a modal filter in nonlinear system identification was successfully employed in [1] where a pseudo modal model was used to capture the nonlinear characteristics of a complex structure. The success of this method is directly dependent on the ability of the modal filter to eliminate all other modal responses except for the single mode of interest. Reference [1] offers multiple methods for modal filtering the measured responses. One of those options, the Full Modal Filter (FMF), is utilized for this work. The FMF is derived from the modal substitution equation:

$$\underline{\ddot{u}} = \underline{\underline{\Phi}} \cdot \underline{\ddot{q}} \tag{1}$$

where $\underline{\underline{\Phi}}$ is the matrix of all rigid body and elastic extracted mode shapes in the frequency band of interest. By pre-multiplying (1) by the pseudo-inverse of the mode shape matrix, one obtains

$$\underline{\underline{\Phi}}^{+} \cdot \underline{\ddot{u}} = \underline{\ddot{q}} \tag{2}$$

The desired modal response is then selected from the corresponding row (or column) of $\underline{\ddot{q}}$. The $\underline{\underline{\Phi}}$ matrix for this work was extracted from the low level impact testing described in Section 4.3. Fig. 3 shows the response of the X translation mode of the steel block extracted from the 311 N impact test. Now that this mode has been isolated, its associated time-varying damping can now be extracted.

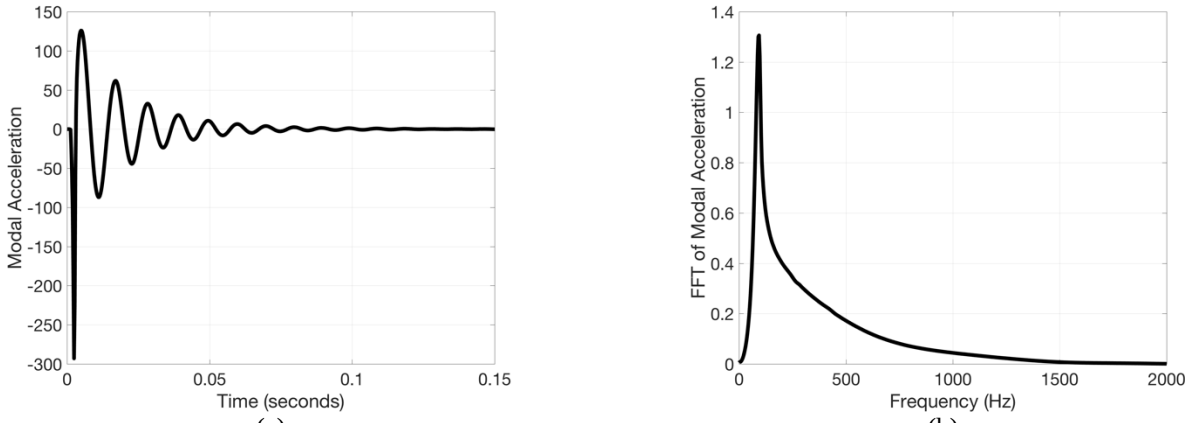

(a) (b)

Fig. 3 Modal acceleration of mode 8 extracted from 311 N impact experiment in (a) time domain and (b) frequency domain

5.2 Nonlinear Damping from Ring-Down Data

Once we have obtained a single degree of freedom response of mode 8 from modal filtering as described above, we can quantify the damping as a function of time. The method for accomplishing this is described in [1] which closely follows the procedure from [3] and [4]. In this work, the Hilbert Transform is computed and a cubic polynomial is fit to the time varying amplitude and phase. This approach fits the modal response of mode 8, $\ddot{q}(t)$, to the following functional form,

$$\ddot{q}(t) = e^{d(t)}\cos[\theta(t)] \tag{3}$$

where $d(t)$ and $\theta(t)$ are each cubic polynomials in time and are, respectively, the decay and phase of the time varying response model. In order to calculate the time-varying damping, the analytic signal, $\ddot{Q}(t)$, is used:

$$\ddot{Q}(t) = \ddot{q}(t) + i\,\mathcal{H}(\ddot{q}(t)) \tag{4}$$

where $\mathcal{H}$ represents a Hilbert Transform. The decay, $d(t)$, is fit to the natural log of the amplitude of the analytic signal, $d(t) = \ln\left|\ddot{Q}(t)\right|$, and the phase, $\theta(t)$, is fit to the unwrapped angle, $\theta(t) = \arg[\ddot{Q}(t)]$.

The phase of the analytic signal gives the oscillation frequency, so the damped natural frequency was defined as its derivative in [3],

$$\omega_d(t) \triangleq \dot{\theta}(t) \tag{5}$$

which one can readily show gives the desired result for a linear time invariant system. Similar expressions can be found for ω_n and ζ.

$$\omega_n(t) \triangleq \left(\omega_d(t)^2 + \dot{d}^2(t)\right)^{\frac{1}{2}} \tag{6}$$

$$\zeta(t) \triangleq \frac{\dot{d}(t)}{\omega_n(t)} \tag{7}$$

The above process was completed for the ring-down response of mode 8 extracted from the 311 N impact data and the time varying damping is plotted in Fig. 4. As a high level verification of this curve, an estimate of the linear damping for this mode was extracted from the 311 N impact data using SMAC and was determined to be 11%. From Table 2, the linear damping for this mode as extracted from a 2 N impact was determined to be 6%. Comparing the achieved damping values from Fig. 4 to the linear approximations of damping at high and low level excitation gives confidence that the time-varying damping extracted from the 311 N is reasonable.

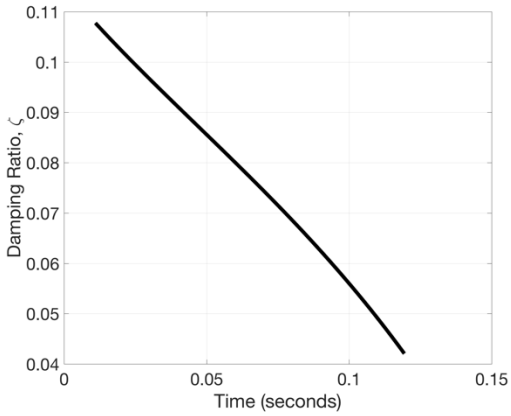

Fig. 4 Time-varying damping for mode 8 extracted from 311 N hammer hit

6 CALIBRATION OF LINEAR FEM

Before the nonlinear damping from Section 5.2 can be incorporated into a FEM, an accurate FEM must first be created for the linear model. The finite element mesh is illustrated in Fig. 5. The mesh consists of 110,938 8-node hexahedral elements and 127,039 nodes. The bolts are represented by beam elements which are connected to the volumetric hexahedral elements through kinematic constraint equations (rigid pseudo-elements) [5]. The mass of the bolts, washers, nuts, and compression sleeves was accounted for by updating the density of the beam element material and the stiffness of the beam element material was increased to reflect the addition of the compression sleeves and the preloaded state of the system. The stiffness properties of the bolts and compression sleeves are not important in this instance since the stiffness need only be high enough to ensure that no strain energy develops in the bolts for the first six modes of the system (i.e. that the first six elastic modes of the assembly are strictly rigid body motion of the steel block, assuring that all strain energy is contained in the silicone pads). The mass properties, however, are very important. Therefore, each component of the experimental system was individually weighed and the density of the corresponding component was appropriately updated in the finite element model.

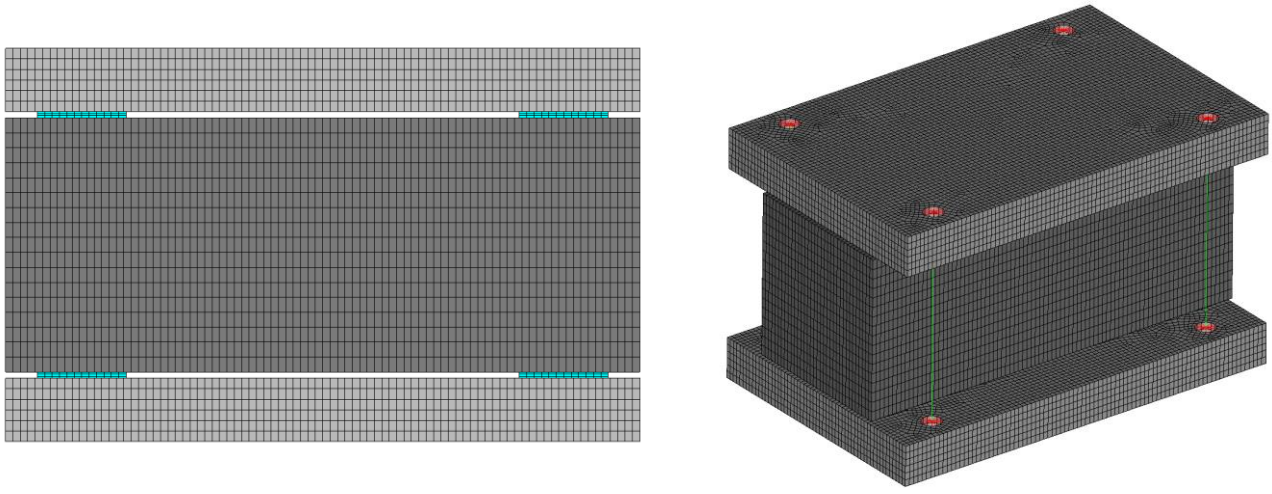

(a) (b)

Fig. 5 (a) Side view and (b) isometric view of the finite element mesh of the system

The corresponding mode shapes and modal frequencies of the system were then estimated using Sierra SD (Structural Dynamics), a massively parallel finite element code developed and maintained by Sandia National Laboratories [6]. If we assume that the cellular silicone material behaves in an elastic, isotropic manner then we have two stiffness parameters with which to calibrate the FEM (the elastic modulus and Poisson's ratio). The calibration was performed with respect to the experimentally obtained mode shapes and modal frequencies from Table 2, and the results are shown in Table 3.

Table 3 Results from Calibration of FEM to Experimentally Extracted Modal Data

Experimental Mode Number	Calibrated FEM Modal Frequency (Hz)	Experimentally Determined Modal Frequency (Hz)	Percent Error
7	104.3	93	12.15%
8	104.3	106	-1.60%
9	114.8	116	-1.03%
10	113.5	127	-10.63%
11	190.5	190	0.26%
12	208.5	209	-0.24%

Note that for modes 7 and 10 there is significant error between the experimentally extracted frequency and that obtained from the FEM. We believe the cause of this discrepancy is the asymmetric pre-loading in the experiment created by additional compression of the lower silicone pads due to gravitational effects; during testing, the bottom pads were visibly more compressed than the top pads due to the weight of the block. This effect was not replicated in the model. However, this work focuses on the motion associated with mode 8 since it deforms the silicone pads solely in shear and was able to be most purely excited in the experiment (see Fig. 6). Therefore, the experiment-FEM discrepancies for modes 7 and 10 do not significantly influence the results presented herein.

Fig. 6 Shape of mode 8

7 DEVELOPMENT OF CONSTITUTIVE DAMPING MODEL

Once the linear FEM was calibrated to the low level impact data, the time-varying damping extracted from the high level experiment was incorporated into the FEM where a simulation of the 311 N impact was conducted. The results from the FEM were then used to derive the constitutive damping model for cellular silicone as a function of shear strain energy. Strain energy was selected since it is a general quantity that is also decaying in time similar to the calculated level of damping. The amplitude of the peaks in strain energy also increases with increases in excitation forces, which is qualitatively consistent with the experimental data. The following two subsections describe the constitutive damping model development process in greater detail.

7.1 Shear Strain-Based Damping Model

In this section we propose allowing the damping ratio for mode 8 to be a function of the current level of strain energy in the cellular silicone material, defined in equation (8). The classical, coupled equations of motion may be written as shown in equation (9).

$$SE_{CS} = \frac{1}{2}\,\underline{u}^T(x,t)\cdot\underline{\underline{K}}_{CS}\cdot\underline{u}(x,t) \tag{8}$$

$$\underline{\underline{M}}\,\underline{\ddot{u}}(x,t) + \underline{\underline{C}}\,\underline{\dot{u}}(x,t) + \underline{\underline{K}}\,\underline{u}(x,t) = \underline{F}(x,t) \tag{9}$$

Let $\underline{u}(x,t) = \sum_{i=1}^{N} q_i(t)\cdot\underline{\varphi}_i$ where $q_i(t)$ is the i^{th} modal coordinate and $\underline{\varphi}_i$ is the i^{th} mass-normalized mode shape. If we employ modal damping and allow the damping ratio to be a function of strain energy in the cellular silicone for a particular shear deformation mode (say mode k), the damping matrix takes on the following form:

$$\underline{\underline{C}} = 2 \cdot \zeta_k(SE_{CS}) \cdot \omega_k \cdot \left(\underline{\underline{M}}\,\underline{\varphi_k}\right) \otimes \left(\underline{\underline{M}}\,\underline{\varphi_k}\right) + \sum_{\substack{i=1 \\ i \neq k}}^{N} 2 \cdot \zeta_i \cdot \omega_i \cdot \left(\underline{\underline{M}}\,\underline{\varphi_i}\right) \otimes \left(\underline{\underline{M}}\,\underline{\varphi_i}\right) \tag{10}$$

Substituting the expression for $\underline{u}(x,t)$ and equation (10) into equation (9) and pre-multiplying the equation by $\underline{\varphi_j}^T$ we obtain the following set of uncoupled modal equations as a result of orthogonality of the modal vectors with respect to $\underline{\underline{M}}$ and $\underline{\underline{K}}$:

$$\begin{aligned} \ddot{q}_i(t) + 2 \cdot \zeta_i \cdot \omega_i \cdot \dot{q}_i(t) + {\omega_i}^2 q_i(t) &= \underline{\varphi_i}^T \underline{F}(x,t) \quad , \; i = 1 \ldots N, \; i \neq k \\ \ddot{q}_i(t) + 2 \cdot \zeta_i(SE_{CS}) \cdot \omega_i \cdot \dot{q}_i(t) + {\omega_i}^2 q_i(t) &= \underline{\varphi_i}^T \underline{F}(x,t) \quad , \; i = k \end{aligned} \tag{11}$$

where the strain dependency of damping is indicated for mode k. Note that for this work, ζ_i is constant and is equal to the corresponding value in Table 2 for all modes except for mode 8. This is an approximation since other modes of the system exercise the silicone pads in shear. However, the 311 N impact primarily excited mode 8, and therefore the responses of the other modes are relatively insignificant.

It is noted that there is also a stiffness nonlinearity; when subjected to the 311-N impact load, the frequency of mode 8 changes from approximately 84 Hz at high amplitude response (early time) to 103 Hz at low amplitude response (late time). However, damping is the focus of this work and as such the natural frequency was assumed constant throughout each simulation and was chosen to match the response frequency in early time for each load level (see Table 4). In order to realize these frequencies in the FEM, the elastic modulus of the cellular silicone was appropriately altered for each load level.

Table 4 Mode 8 Simulation Natural Frequencies

Experimental Input Load Level (N)	FEM Simulation Natural Frequency (Hz)
44	94
178	92
311	88

7.2 FEM Simulation

Since strain energy is not easily extracted from nonlinear experimental data, the relationship between shear strain energy and damping was developed using the FEM by simulating the response of mode 8 to the equivalent modal force produced by the 311 N impact where the natural frequency was held constant at 88 Hz and the modal damping versus time data from Fig. 4 was used directly. The results are presented in Fig. 7. It is clear that the modal acceleration amplitude prediction shows very good agreement with the experimental measurement. This provides additional confidence in the measured damping ratio versus time data.

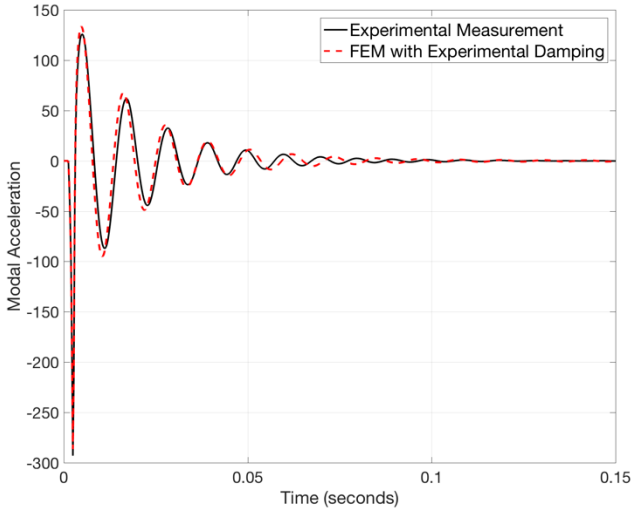

Fig. 7 Measured modal acceleration vs. prediction using measured damping ratio versus time data for mode 8 (311 N load)

The FEM-computed shear strain energy versus time for this same simulation run is shown in Fig. 8. By plotting the measured damping ratio versus the amplitude of each peak in shear strain energy and applying a curve fit to the data we arrive at the

empirically-derived, constitutive damping model for damping as a function of strain energy in the cellular silicone material. The data and curve fit are shown in Fig. 9 and the curve fit equation is provided in (12). This equation was obtained by applying a simple fourth order polynomial fit of the base 10 logarithm of the data. The equation form was selected so that the damping ratio would remain positive and approach zero as the strain energy approaches zero.

$$\zeta(SE_{CS}) = 10^{(-0.0034234\cdot\log_{10}(SE_{CS})^4 - 0.042199\cdot\log_{10}(SE_{CS})^3 - 0.19624\cdot\log_{10}(SE_{CS})^2 - 0.3451\cdot\log_{10}(SE_{CS})^1 - 1.1678)} \quad (12)$$

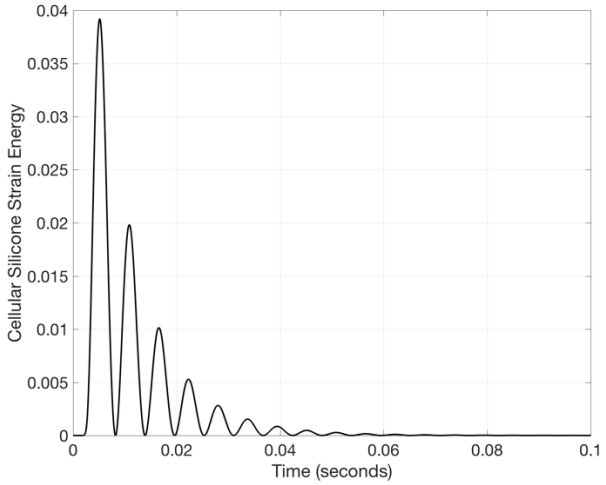

Fig. 8 Computed strain energy vs. time in the cellular silicone material when subjected to the 311 N load

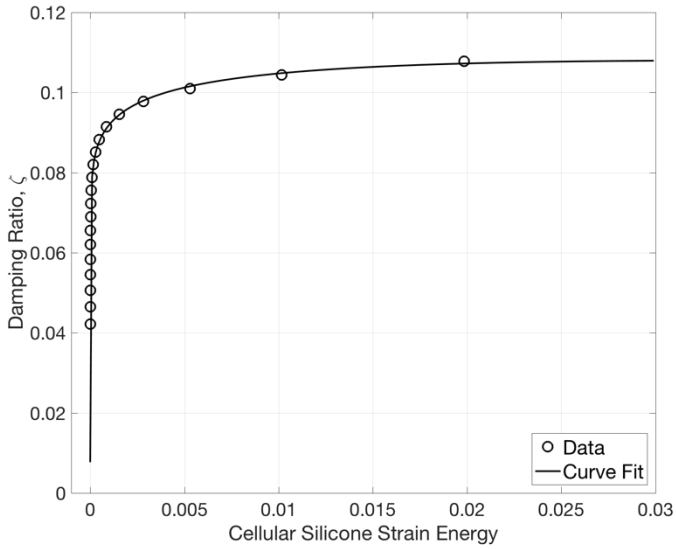

Fig. 9 Damping ratio for mode 8 versus strain energy amplitude in the cellular silicone material

As an initial check on the efficacy of this developed constitutive damping property, (12) was used to predict the response of mode 8 to the equivalent modal force from the 44-N and 178-N impacts. In order to incorporate (12) into the solution (which depends on the calculation of the strain energy in only the cellular silicone at every time step) the C++ finite element library, deal.II [7] and the SLEPc eigensolver [8] were used. The former was utilized to assemble the mass and stiffness matrices from which the SLEPc eigensolver then extracted the corresponding modal frequencies and mode shapes. Note that these modal frequencies were within 1-2Hz of those calculated by Sierra SD as described in Section 6. The mode shapes were used to obtain the modal force that was applied in each simulation.

There were two strategies employed for updating the damping ratio while numerically integrating the single modal equation for comparison to the test data. The first strategy involved continuously updating the damping ratio by computing the current

strain energy in the cellular silicone at every time step. The second involved only updating the damping ratio at peaks in strain energy. This latter method was studied since the original damping ratio versus strain energy data was really damping ratio versus the *peaks* in the computed strain energy. Thus, it seems reasonable to only update the damping ratio at peaks in the strain energy. The modal acceleration response prediction results obtained for the 178-N and 44-N loads are illustrated in Fig. 10 and Fig. 11, respectively.

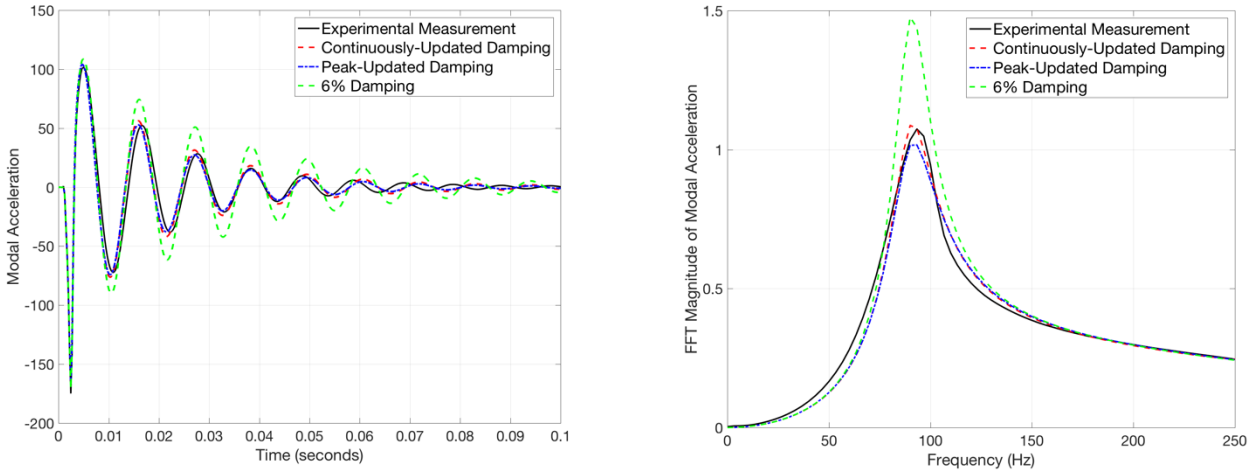

(a) (b)

Fig. 10 (a) Modal acceleration prediction vs. experimental data in the time domain and (b) frequency domain, 178 N hit

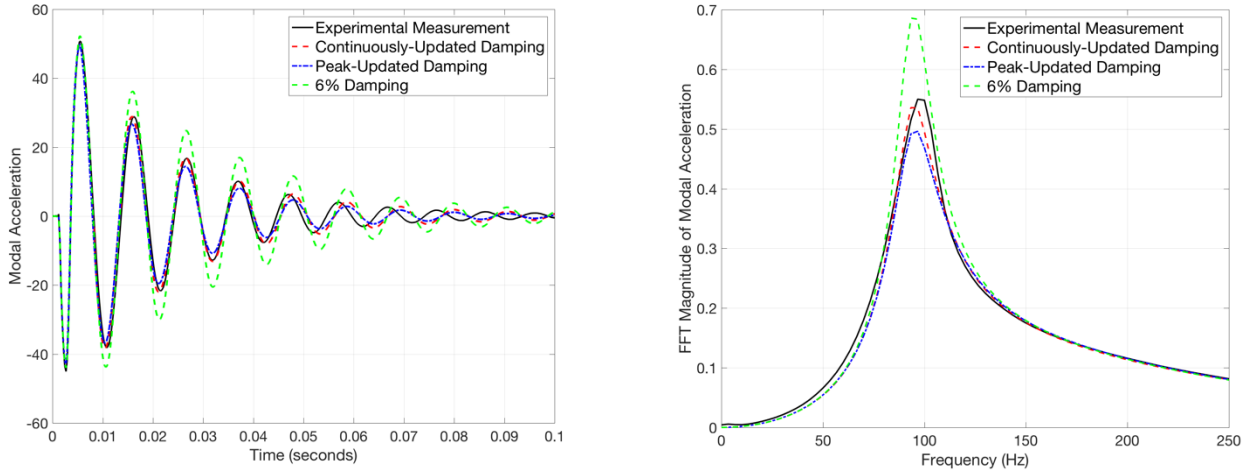

(a) (b)

Fig. 11 (a) Modal acceleration prediction vs. experimental data in the time domain and (b) frequency domain, 44 N hit

Relative to the results from the linear, experimentally extracted damping estimate from mode 8, the results from the continuously-updated and peak-updated damping values are encouraging. Fig. 10b and Fig. 11b illustrate approximately the same character of the response. Since the amplitude of the strain energy in the pads is decreasing in time, the peak-updated damping removes slightly more energy in each cycle since it keeps the damping constant over the cycle. Consequently, the amplitude of the modal acceleration response in this case is slightly under-predictive. In contrast, the predicted response using continuously-updated damping appears to result in significantly more accurate energy dissipation characteristics as evidenced by the improved response amplitude prediction. For reference, the maximum strain energy produced by the 311, 178, and 44 N loads correspond to values of 0.02, 0.01, and 0.003, respectively (refer to Fig. 9).

8 CONCLUSIONS

The results from experimental testing were used in order to derive a constitutive damping model for cellular silicone as a function of strain energy for deformations primarily involving shear. It was demonstrated that the results for the same system subjected to two different levels of load are encouraging. However, additional testing is necessary in order to confirm

whether the method can be generalized to improve the predictive accuracy of a system with mode shapes containing strain energy in multiple components in addition to shear strain in the cellular silicone.

9 PLANS FOR FUTURE WORK

The presented development in this paper may only be applicable for mode shapes in which shear is the primary deformation mode in the cellular silicone. This is evidenced by the linear damping extraction for each of the first six flexible modes provided in Table 2. The modes involving primarily tensile/compressive deformation are associated with much higher levels of damping than the those associated with primarily shear deformation. Thus, we plan to develop a similar damping constitutive model for modes involving primarily deformation along the axis of preload by applying the same process to mode 11.

Since we were not able to complete additional testing with a different system, it is still uncertain whether this approach to apply modal damping would improve accuracy in a general setting. Currently, we plan to modify the test fixture geometry in order to determine whether this method improves the predictive capability of a linear FEM for a different assembly and input load. Furthermore, if we are successful, we would like to try to incorporate a modified version of this approach into a model of an assembly in which multiple modes with significant strain energy in numerous components in addition to the cellular silicone are excited by a single input load.

10 REFERENCES

[1] Mayes, R. L., Pacini, B.R., Roettgen, D.R., "A Modal Model to Simulate Typical Structural Dynamic Nonlinearity," presented at the 34th International Modal Analysis Conference Orlando, Florida, 2016.

[2] Hensley, Daniel P., Mayes, Randy L., “Extending SMAC to Multiple References”, Proceedings of the 24th International Modal Analysis Conference, pp 220-230, January 2006

[3] B. Deaner, Allen, M. S., Starr, M.J., Segalman, D.J., and Sumali, H., "Application of Viscous and Iwan Modal Damping Models to Experimental Measurements From Bolted Structures," *ASME Journal of Vibration and Acoustics*, vol. 137, 2015 2015.

[4] M. W. Sracic, *et al.*, "Identifying the modal properties of nonlinear structures using measured free response time histories from a scanning laser Doppler vibrometer," presented at the 30th International Modal Analysis Conference Jacksonville, Florida, 2012.

[5] Reese, G., Bhardwaj, M., and Walsh, T., “Sierra Structural Dynamics – Theory Manual”, Technical Report SAND2009-0748, Sandia National Laboratories, 2011

[6] Sierra Structural Dynamics Development Team, “Sierra Structural Dynamics – User’s Notes”, Technical Report SAND2015-9132, Sandia National Laboratories, 2015.

[7] Bangerth, W., Davydov, D., Heister, T., Heltai L., Kanschat, G., Kronbichler, M., Maier, M., Turcksin, B., and Wells, D., “The deal.II Library, Version 8.4”, Journal of Numerical Mathematics, Vol. 24, 2016

[8] Hernandez, V., Roman, J., and Vidal, V. “SLEPc: A scalable and flexible toolkit for the solution of eigenvalue problems”, ACM Trans. Math. Software, 31(3):351-362, 2005